Stability-Considered Lane Keeping Control of Commercial Vehicles Based on Improved APF Algorithm

Bin Tang (tangbin@ujs.edu.cn)
Jiangsu University https://orcid.org/0000-0002-1520-0625
Zheng-Yi Yang
Jiangsu University
Hao-bin Jiang
Jiangsu University
Zi-yan Lin
Jiangsu University
Zhan-xiang Xu
Jiangsu University
Zi-tian Hu
Jiangsu University

Original Article

Keywords: Lane keeping control, Commercial vehicles, Lateral stability, Artificial potential field, AIWPSO

Posted Date: June 30th, 2021

DOI: https://doi.org/10.21203/rs.3.rs-652627/v1

Title page

Stability-considered Lane Keeping Control of Commercial Vehicles based on Improved APF Algorithm

Bin Tang received the B.S. degree in electronics and information engineering, and the M.S. and Ph.D. degrees in vehicle engineering from *Jiangsu University*, *Zhenjiang*, *China*, in 2007, 2011, and 2015, respectively. He is currently an associate professor with the *Automotive Engineering Research Institute*, *Jiangsu University*. His research interests include vehicle handling dynamics and control, intelligent steering, electric motor drive and control.
Tel: 0511-88782845; E-mail: tangbin@ujs.edu.cn

Zheng-Yi Yang received the B.S. degree in traffic equipment and control engineering from *Nantong University*, *Nantong*, *China*, in 2020. She is currently a postgraduate student in the *Automotive Engineering Research Institute*, *Jiangsu University*, majored in vehicle engineering. Her research interest is lane keeping control.

Hao-Bin Jiang received the B.S. degree from *Nanjing Agricultural University*, *Nanjing*, *China*, in 1991, and the M.S., and Ph.D. degrees from *Jiangsu University*, *Zhenjiang*, *China*, in 1994 and 2000, respectively, all in mechanical engineering. He is currently a professor with the *School of Automotive and Traffic Engineering*, *Jiangsu University*. His research interests include vehicle dynamics performance analysis and electronic control technologies for vehicles.

Zi-Yan Lin received the B.S. degree in vehicle engineering from *Jiangsu University*, *Zhenjiang*, *China*, in 2018. He is currently a postgraduate student in the *Automotive Engineering Research Institute*, *Jiangsu University*, majored in vehicle engineering. His research interest is intelligent steering control.

Zhan-Xiang Xu received the B.S. degree in vehicle engineering from *Anhui University of Science and Technology*, *Huainan*, *China*, in 2019. He is currently a postgraduate student in the *Automotive Engineering Research Institute*, *Jiangsu University*, majored in vehicle engineering. His research interest is path planning and tracking.

Zi-Tian Hu received the B.S. degree in vehicle engineering from *Nanhang Jincheng College*, *Nanjing*, *China*, in 2020. He is currently a postgraduate student in the *Automotive Engineering Research Institute*, *Jiangsu University*, majored in vehicle engineering. His research interest is intelligent vehicle decision-making and planning.

Corresponding author：Bin Tang　E-mail：tangbin@ujs.edu.cn

Stability-considered Lane Keeping Control of Commercial Vehicles based on Improved APF Algorithm

Bin Tang[1], Zheng-Yi Yang[1], Hao-Bin Jiang[2], Zi-Yan Lin[1], Zhan-Xiang Xu[1], Zi-Tian Hu[1]

Abstract: With regard to the lane keeping system, path tracking accuracy and lateral stability at high speeds need to be taken into account especially for commercial vehicles due to the characteristics of larger mass, longer wheelbase and higher mass center. To improve the performance mentioned above comprehensively, the control strategy based on improved artificial potential field (APF) algorithm is proposed. In the paper, time to lane crossing (TLC) is introduced into the potential field function to enhance the accuracy of path tracking, meanwhile the vehicle dynamics parameters including yaw rate and lateral acceleration are chosen as the repulsive force field source. The lane keeping controller based on improved APF algorithm is designed and the stability of the control system is proved based on Lyapunov theory. In addition, adaptive inertial weight particle swarm optimization algorithm (AIWPSO) is applied to optimize the gain of each potential field function. The co-simulation results indicate that the comprehensive evaluation index respecting lane tracking accuracy and lateral stability is reduced remarkably. Finally, the proposed control strategy is verified by the HiL test.

Keywords: Lane keeping control • Commercial vehicles • Lateral stability • Artificial potential field • AIWPSO

✉ Bin Tang
tangbin@ujs.edu.cn

[1] Automotive Engineering Research Institute, Jiangsu University, Zhenjiang 212013, China

[2] School of Automotive and Traffic Engineering, Jiangsu University, Zhenjiang 212013, China

1 Introduction

With the rapid development of high-level highway networks and modern transportation industry, the traffic accidents of commercial vehicles are obviously increased, among which 20% of traffic accidents are caused by lane departure statistically [1–2]. Advanced driver assistance systems (ADAS) have emerged as an efficient way of reducing traffic accidents and improving driving comfort[3–5], which is also an inevitable stage in the development of autonomous vehicles (AVs). As an important part of ADAS[6], lane keeping system (LKS) helps drivers to regulate driving direction automatically when lane departure is detected, thus alleviates the driving fatigue and improves the driving safety[7], which attracts more attentions of several researchers.

Path tracking control is one of the most important research aspects of LKS, in which the control objective is to ensure the lane tracking errors such as lateral deviation and course deviation approach to zero[8–9]. Many advanced control algorithms have been applied in LKS controller design to achieve accurate lane tracking, such as robust control[10, 11], model predictive control[12], sliding mode control[13], fuzzy control[14]. Most of the algorithms mentioned above are model-based or deviation-based algorithms. The model-building errors and external input disturbance may affect the control accuracy. On the other hand, especially at high speed, above algorithms cannot function well in the aspect of path tracking due to time delay and the fragility of algorithms themselves in a complex environment.

Artificial potential field (APF) algorithm is favored by many scholars in the area of vehicle dynamics control

[15–16] due to its visualized mathematical presentation and strong control ability in complex dynamic environments. Besides, the potential field item can be increased according to the different requirements and the algorithm can be combined with the vehicle dynamics. APF algorithm has been also applied in the lane keeping control by some researchers. In [17], Rossetter carried out the research about Lyapunov based performance guarantees for the potential field lane-keeping assistance system. In [18], Wang Qidong et al. proposed a lane keeping control method based on parameter-varying artificial potential field. It can be found from previous researches that the gravitational field is constructed only based on the pre-sight deviation in traditional road artificial potential field algorithm, which leads to long regulation time and poor tracking accuracy in the process of lane keeping for commercial vehicles. In addition, the lateral stability in the lane keeping process is another significant concern. There is no doubt that commercial vehicles are more prone to be instable due to higher center of mass, larger mass and longer wheelbase[19]. According to statistics, 20% of commercial vehicle accidents are caused by lateral roll and lateral instability, 66% of which occur during the turning process [20]. Therefore, it is of great significance to take above two problems into consideration comprehensively. From this viewpoint, in this study, the improved APF controller is designed to generate the target front wheel angle, which combines road environment information with vehicle dynamics parameters to deduce new potential field function.

In the improved APF controller, the gains in the potential field function play an important role in system stability and lane keeping performance. In this paper, adaptive inertia weight particle swarm optimization (AIWPSO) algorithm is applied to optimize the gains in the potential field function taking the comprehensive evaluation index including path tracking accuracy and lateral stability as the optimization function, and taking the result of stability demonstration based on Lyapunov methodology as the constraints. AIWPSO algorithm is an improvement of PSO algorithm through adaptive adjustment of inertia weight, which is beneficial to realize rapid convergence of algorithm and improve global search capability[21].

The paper is organized as follows. Models of vehicle dynamics is constructed in Section 2. The design and stability analysis of lane keeping controller based on improved APF are carried out in Section 3. In Section 4, comprehensive evaluation index is established and the controller parameters are optimized based on AIWPSO algorithm. Simulations and HiL tests are carried out in Section 5 to verify the proposed control strategy based on improved APF algorithm. Followed are the conclusions in the Section 6.

2 Vehicle Dynamics Modeling

A three-degree-of-freedom（3 DOF）dynamics model of the commercial vehicle is built in this paper as a reference model for the controller as shown in Figure 1. In the model, the front wheel angle δ_f is taken as the input variable. β and ω_r represent the sideslip angle and yaw rate, respectively. The generalized lateral tire forces are denoted by F_{xi} and $F_{yi}(i=1,2,3,4)$, where we have $F_{yf}=F_{y1}+F_{y2}$ and $F_{yr}=F_{y3}+F_{y4}$.According to the linear tire model, we have $F_{yf}=-k_f\cdot\alpha_f$ and $F_{yr}=-k_r\cdot\alpha_r$.

Based on parallel axis theorem, the relationship between the roll inertia moment I_x and the inertia moment I_{xeq} about the roll axis through the C.G. of the sprung mass m_s is described as $I_{xeq}=I_x+m_sh_g^2$.To simplify the controller design, it is assumed that $\sin\phi\approx\phi$, $\cos\phi\approx0$, and β is small enough. Given a vehicle with total mass m, yaw inertia moment I_z and roll inertia moment I_x, the equations of vehicle dynamics are obtained in Eq.(1)[22].

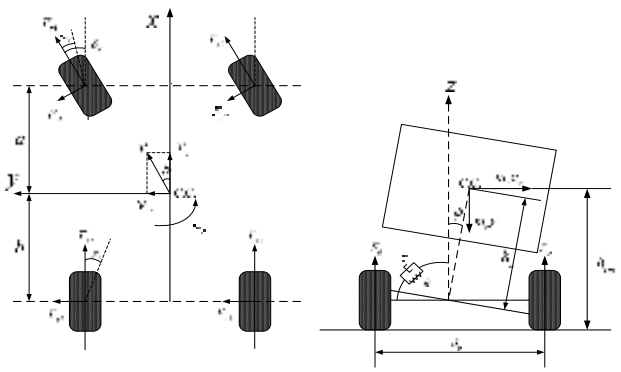

Figure 1 3-DOF dynamics model of the commercial vehicle

$$\begin{cases} m\dot{v}_y=-k_r\dfrac{v_y-\omega_r b}{v_x}-k_f\dfrac{v_y+\omega_r a}{v_x}-m\omega_r v_x+m_sh_g\ddot{\phi}+k_f\delta_f \\ I_Z\dot{\omega}_r=-ak_f\dfrac{v_y+\omega_r a}{v_x}+bk_r\dfrac{v_y-\omega_r b}{v_x}+ak_f\delta_f \\ I_{xeq}\ddot{\phi}=ma_yh_g+m_sgh_g\phi-c\dot{\phi}-k\phi \end{cases} \tag{1}$$

where k_f,k_r represent cornering stiffness of the front and rear wheel respectively, k is the equivalent roll stiffness of

suspension, c is the equivalent damping coefficient of suspension, ϕ is the roll angle, $\dot{\phi}$ is the roll rate, h_g refers to the distance from center of mass to roll center.

After transformation, we have the following state-space equation

$$\dot{X} = AX + Bu, \tag{2}$$

where A, B are coefficient matrix, δ_f is the control input variable and state variable is chosen as $X = [v_y \quad \omega_r \quad \dot{\phi} \quad \phi]^{\mathrm{T}}$. The coefficient matrix can be given as follows.

$$A = \begin{bmatrix} -\dfrac{(k_f + k_r)I_{xeq}}{mI_x v_x} & \dfrac{(bk_r - ak_f)I_{xeq}}{mI_x v_x} - v_x & \dfrac{-m_s h_g c}{mI_x} & \dfrac{m_s h_g (mgh_g - k)}{mI_x} \\ \dfrac{bk_r - ak_f}{I_z} & \dfrac{b^2 k_r + a^2 k_f}{I_z v_x} & 0 & 0 \\ \dfrac{-h_g(k_f + k_r)}{I_x} & \dfrac{h_g(bk_r - ak_f)}{I_z v_x} & \dfrac{-c}{I_x} & \dfrac{mgh_g - k}{I_x} \\ 0 & 0 & 1 & 0 \end{bmatrix}$$

$$B = \begin{bmatrix} \dfrac{I_{xeq}k_f}{mI_x} & \dfrac{ak_f}{I_z} & \dfrac{h_g k_f}{I_x} & 0 \end{bmatrix}^{\mathrm{T}}$$

3 Stability-considered Lane Keeping Control Strategy

3.1 Overall Control Strategy

The improved artificial potential field (APF) algorithm is applied to design the overall control strategy, including new potential field function construction considering vehicle stability, establishment of comprehensive evaluation index and controller parameter optimization based on adaptive inertia weight particle swarm optimization (AIWPSO) algorithm. The overall control schematic diagram is shown in Figure 2. The controller outputs the target front wheel angle and the electro-hydraulic hybrid power steering (EHHPS) system realizes the tracking of the target front wheel angle. From the steering system, the real front wheel angle is transmitted to the vehicle model in Trucksim software. The vehicle dynamics parameters and lane line information from the vehicle model are the inputs of the potential field function in the lane keeping controller and then a closed-loop lane keeping control is carried out.

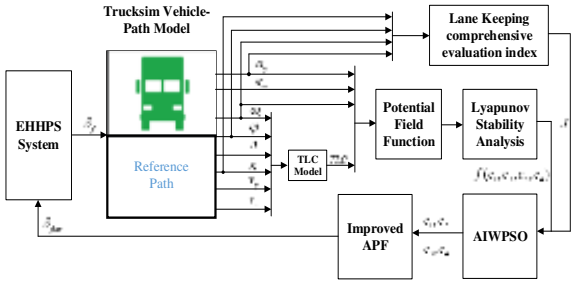

Figure 2 The schematic of lane keeping control system

3.2 Design of The Improved APF Controller

As is presented in chapter 2, the vehicle dynamics model can also be described as the following form.

$$M\dot{X} = HX + G_1, \tag{3}$$

Wherein,

$$G_1 = G\delta_f$$

$$M = \begin{bmatrix} m & 0 & 0 & 0 \\ 0 & I_z & 0 & 0 \\ 0 & 0 & I_{xeq} & 0 \\ 0 & 0 & 0 & 1 \end{bmatrix}, \quad G = \begin{bmatrix} \dfrac{I_{xeq}k_f}{I_x} \\ ak_f \\ \dfrac{h_g I_{xeq} k_f}{I_x} \\ 0 \end{bmatrix}$$

$$H = \begin{bmatrix} -\dfrac{(k_f + k_r)I_{xeq}}{I_x v_x} & \dfrac{(bk_r - ak_f)I_{xeq}}{I_x v_x} - mv_x & \dfrac{-m_s h_g c}{I_x} & \dfrac{m_s h_g (mgh_g - k)}{I_x} \\ \dfrac{bk_r - ak_f}{v_x} & \dfrac{b^2 k_r + a^2 k_f}{v_x} & 0 & 0 \\ \dfrac{-h_g I_{xeq}(k_f + k_r)}{I_x} & \dfrac{h_g I_{xeq}(bk_r - ak_f)}{I_z v_x} & \dfrac{-I_{xeq}c}{I_x} & \dfrac{mgh_g I_{xeq} - kI_{xeq}}{I_x} \\ 0 & 0 & 1 & 0 \end{bmatrix}$$

$$G_1 = G_d + G_v = \begin{bmatrix} \dfrac{I_{xeq}k_f}{I_x} \\ ak_f \\ \dfrac{h_g I_{xeq} k_f}{I_x} \\ 0 \end{bmatrix} \delta_f = \begin{bmatrix} \dfrac{I_{xeq}k_f}{I_x} \\ ak_f \\ \dfrac{h_g I_{xeq} k_f}{I_x} \\ 0 \end{bmatrix} \delta_d - \begin{bmatrix} \dfrac{I_{xeq}k_f}{I_x} \\ ak_f \\ \dfrac{h_g I_{xeq} k_f}{I_x} \\ 0 \end{bmatrix} \cdot \sum_{i=1}^{n} \frac{\partial V_i}{\partial x_i}$$

In Eq. (3), the first two items M and H are related to the inherent properties of the vehicle, and the last item G_1 is the control item determined by the external inputs, which is mainly composed of driver input item G_d and potential field function control item G_v, in which the force of potential field is the partial derivative of each potential

field with respect to the potential field variable and the direction points to the lane center line.

When the vehicle is at the centerline, there is no lateral deviation and the potential field function control item G_v has almost no influence on the vehicle which is mainly controlled by the driver input item G_d . When the vehicle deviates, the controller will enable the lane keeping function, which is completely controlled by the potential field function control item G_v , namely G_d =0. By substituting the vehicle dynamics model into the potential field function, the target front wheel angle can be obtained by Eq. (4).

$$\delta_{f\text{tar}} = -\frac{1}{k_f}\sum_{i=1}^{n}\frac{\partial V_i}{\partial x_i}, \tag{4}$$

3.3 Establishment of Improved APF Function

As a virtual force method, the basic principle of the artificial potential field method is to construct artificial potential field function and represent the influence of vehicle risk level in the lane environment. Due to the low control accuracy of the traditional road artificial potential field and the instability of commercial vehicles, in this paper, the potential field function is improved on the basis of the traditional road APF, which introduces TLC, yaw rate ω_r and lateral acceleration a_y into the function to construct the virtual repulsion potential field.

3.3.1 Road Artificial Potential Field Function

The road artificial potential field represents risk level of the vehicle in different areas of the lane. The motion direction of the vehicle in the artificial potential field is consistent with the declining direction of the potential field[23]. The road artificial potential field takes the lateral deviation of the preview point as the variable of potential field. The schematic of driver's preview is shown in Figure 3. When the vehicle moves, the centerline has certain gravitation on the vehicle by the potential field, and the gravitation force increases with the deviation. The gravitation force is the largest at the edge of the lane and the gravitation force is 0 at the centerline. The road artificial potential field function designed in this paper is a quadratic function shown in Eq.(5).

$$V_{e_{la}} = c_1 e_{la}^{\ 2} = c_1[e + (x_{cf} + x_{la})\sin\varphi]^2, \tag{5}$$

Where c_1 is the gain of artificial gravitational potential field function, e is the lateral deviation between the vehicle's center of mass and the lane centerline, x_{cf} is the distance from the center of mass to the action point of the potential field force, x_{la} is the preview distance, φ is heading angle.

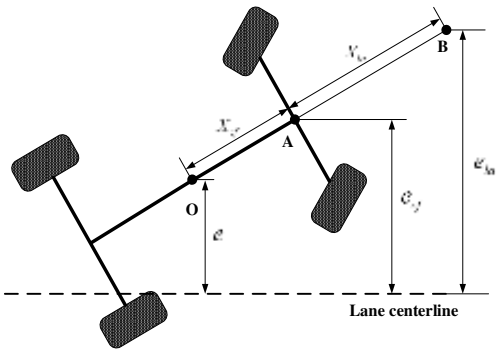

Figure 3 Diagram of driver's preview

3.3.2 TLC Artificial Potential Field Function

Time to lane crossing (TLC) is an important parameter to judge whether the vehicle will deviate the lane. In this paper, TLC is introduced to establish a potential field function shown as follows.

$$V_{TLC} = c_2\left(\frac{1}{\tau_{\max} - \tau} - \frac{1}{\tau_{\max}}\right)^2, \tag{6}$$

Wherein,

$$\tau = 1/TLC$$

$$1/\tau_{\max} = \frac{v_y}{a_{y\max}} + t_2$$

Where c_2 is the gain of artificial potential field function of TLC, $1/\tau_{\max}$ is the threshold of TLC, which is time-varying with vehicle adjustment time t_1 , vehicle response time t_2 and driver response time t_3 .

Due to the complexity of TLC calculation, TLC artificial potential field function is simplified and the control variable regarding TLC artificial potential field is given in Eq. (7) to facilitate the stability proof.

$$\delta_{\text{TLC}} = -\frac{c_2}{k_f}\tau[\text{sgn}(\tau - \tau_{\max}) + 2], \tag{7}$$

3.3.3 Yaw Rate Artificial Potential Field Function

In this paper, yaw rate is introduced into the artificial potential field. The limit of yaw rate ω_μ under the condition of critical instability is the potential field source

to construct the repulsion field. The artificial potential field function of yaw rate is shown as follows in Eq. (8).

$$V_{\omega_r} = c_3(\frac{1}{\omega_\mu - \omega_r} - \frac{1}{\omega_\mu})^2, \quad (8)$$

Wherein,

$$\omega_\mu = 0.85\frac{\mu g}{v_x}$$

where c_3 is the gain of artificial potential field function of yaw rate, ω_r is the yaw rate, ω_μ is the limit of yaw rate, μ is the road adhesion coefficient.

3.3.4 Lateral Acceleration Artificial Potential Field Function

It is known that the front wheel angle has great influence on the lateral acceleration, and sharp variation of front wheel angle is likely to result in the vehicle rollover[24]. The lateral acceleration, in this paper, is introduced into the artificial potential field to avoid the vehicle rollover resulted from excessive lateral acceleration. The maximum lateral acceleration of critical rollover is the potential field source to construct the repulsion field. The artificial potential field function of lateral acceleration is presented in Eq. (9).

$$V_{ay} = c_4(\frac{1}{a_{y\max} - a_y} - \frac{1}{a_{y\max}})^2, \quad (9)$$

Where c_4 is the gain of artificial potential field function of lateral acceleration, $a_{y\max}$ is the maximum lateral acceleration of critical rollover.

3.3.5 Lane Keeping Controller based on APF

Combining the artificial potential field functions mentioned above, the general artificial potential field function is presented in Eq. (10).

$$V = V_{e_{la}} + V_{TLC} + V_{\omega r} + V_{ay} = c_1[e + (x_{cf} + x_{la})\sin\varphi]^2 + c_2(\frac{1}{\tau_{\max} - \tau} - \frac{1}{\tau_{\max}})^2 + c_3(\frac{1}{\omega_\mu - \omega_r} - \frac{1}{\omega_\mu})^2 + c_4(\frac{1}{a_{y\max} - a_y} - \frac{1}{a_{y\max}})^2, \quad (10)$$

The output of lane keeping controller is shown in Eq.(11).

$$\delta_{ftar} = -\frac{1}{k_f}(c_1\frac{\partial V_{ela}}{e_{la}} + c_3\frac{\partial V_{\omega r}}{\omega_r} + c_4\frac{\partial V_{ay}}{a_y}) + \delta_{TLC}, \quad (11)$$

3.4 Lyapunov-based proof of controller stability

Lyapunov function for the control system shown in Eqs.(12)~(13) is constructed by the vehicle's kinetic energy and a new potential energy-like term [25].

$$L = T_1 + V_1, \quad (12)$$

Wherein,

$$T_1 = \frac{1}{2}mv_y^2 + \frac{1}{2}I_z\omega_r^2 + \frac{1}{2}I_{xeq}\dot{\phi}^2, \quad (13)$$

where T_1 is vehicle's kinetic energy of three free degrees of lateral, yaw and roll.

Because TLC potential field function is simplified and integrated into the controller directly, it can be ignored in the stability proof. Therefore, the new potential energy-like term is constructed in Eq. (14).

$$V_1 = V_{e_{la1}} + V_{\omega r} + V_{ay}, \quad (14)$$

where V_{ela1} is reconstructed as Eq.(15).

$$V_{ela1} = c_1e^2 + 2c_1x_{cf}e\varphi + c_1x_{cf}(x_{la} + x_{cf})\varphi^2, \quad (15)$$

In order to implement the system stability proof, the following criteria need to be met.

Criteria I: $L > 0$ and Criteria II: $\dot{L} \le 0$.

The criteria I can be demonstrated by verifying that the kinetic energy and potential energy are both positive. It is obvious that the kinetic energy T, potential energy items $V_{\omega r}$ and V_{ay} are positive if only c_3 and c_4 are positive. It needs to be checked whether the potential energy item V_{ela1} is positive. Converted into the matrix format, V_{ela1} is given by $V_{ela1} = q_0^T V_n q_0$, where $q_0 = [e \quad \varphi]^T$ and the matrix V_n is presented as follows.

$$V_n = \begin{bmatrix} c_1 & c_1x_{cf} \\ c_1x_{cf} & c_1x_{cf}(x_{la} + x_{cf}) \end{bmatrix}$$

Based on Sylvester's theorem, a necessary and sufficient condition for a matrix to be positive definite is for all the principal minors to be strictly positive, so $|V_n| > 0$ only if $x_{cf}x_{la} > 0$. By definition the condition

must be met when c_3 and c_4 are more than 0.

To meet Criteria II, the derivative of Eq. (12) needs to be obtained. $\dot{E}$ is divided into $\dot{T}_1+\dot{V}_{ela1}$ and $\dot{V}_{\omega r}+\dot{V}_{ay}$ to be proved respectively as is shown in Eq. (16).

$$\dot{E}=\dot{T}_1+\dot{V}_1=(\dot{T}_1+\dot{V}_{ela1})+(\dot{V}_{\omega r}+\dot{V}_{ay}), \tag{16}$$

Wherein,

$$\dot{T}_1+\dot{V}_{ela1}=mv_y\dot{v}_y+I_z\omega_r\dot{\omega}_r+I_x\phi\dot{\phi}-2c_1x_{la}\varphi^2v_x-2c_1x_{la}\varphi v_y$$

Combining with 3-DOF vehicle dynamics model, after arrangement, Eq. (17) can be obtained.

$$\begin{aligned}\dot{T}_1+\dot{V}_{ela1}=&v_y\{-\frac{(k_1+k_2)I_{xeq}}{I_xv_x}v_y-[\frac{(ak_1-bk_2)I_{xeq}}{I_xv_x}\\&+mv_x]\omega_r-\frac{m_sh_gc}{I_x}\dot{\phi}+\frac{(mgh_g-k)m_sh_g}{I_x}\phi\}+\\&\dot{\phi}[-\frac{I_{xeq}h_g}{I_x}(k_1+k_2)\frac{v_y}{v_x}-\frac{I_{xeq}h_g}{I_x}(k_1a-k_2b)\frac{\omega_r}{v_x}\\&-\frac{I_{xeq}c}{I_x}\dot{\phi}+\frac{(mgh_g-k)I_{xeq}}{I_x}\phi]+\omega_r[-\frac{a^2k_1+b^2k_2}{v_x}\omega_r\\&-\frac{(ak_1-bk_2)}{v_x}v_y]-2c_1x_{la}\varphi^2v_x-2c_1x_{la}\varphi v_y\end{aligned}, \tag{17}$$

The above equation is transformed into a matrix form as shown in Eq. (18).

$$\dot{E}_{T_1+ela}=-q_1^{\mathrm{T}}Pq_1, \tag{18}$$

where $q_1=\begin{bmatrix}v_y & \omega_r & \dot{\phi} & \varphi & \phi\end{bmatrix}^{\mathrm{T}}$ and matrix P is given as

$$P=\begin{bmatrix}\varsigma_{p11} & \varsigma_{p12} & \varsigma_{p13} & c_1x_{la} & \varsigma_{p51}\\ \varsigma_{p21} & \varsigma_{p22} & \varsigma_{p23} & 0 & 0\\ \varsigma_{p31} & \varsigma_{p32} & \varsigma_{p33} & 0 & \varsigma_{p35}\\ c_1x_{la} & 0 & 0 & 2c_1x_{la}v_x & 0\\ \varsigma_{p15} & 0 & \varsigma_{p53} & 0 & 0\end{bmatrix}$$

with

$$\varsigma_{p11}=\frac{(k_1+k_2)I_{xeq}}{I_xv_x};\varsigma_{p12}=\varsigma_{p21}=\frac{(k_1a-k_2b)}{2v_x}(1+\frac{I_{xeq}}{I_x})+\frac{mv_x}{2}$$

$$\varsigma_{p22}=\frac{a^2k_1+b^2k_2}{v_x};\varsigma_{p13}=\varsigma_{p31}=\frac{I_{xeq}h_g(k_1+k_2)}{2I_xv_x}+\frac{m_sh_gc}{2I_x}$$

$$\varsigma_{p33}=\frac{I_{xeq}c}{I_x};\varsigma_{p32}=\varsigma_{p23}=\frac{I_{xeq}h_g(k_1a-k_2b)}{2I_xv_x}$$

$$\varsigma_{p35}=\varsigma_{p53}=-\frac{(mgh_g-k)I_{xeq}}{2I_x}$$

$$\varsigma_{p15}=\varsigma_{p51}=-\frac{(mgh_g-k)m_sh_g}{2I_x}$$

Only when the matrix P is proved to be nonnegative definite, in other words, the determinants of every order sequential principal minors are not less than 0, $\dot{E}_{T_1+ela}\le 0$ can be met. Owing to ς_{p11} is greater than 0, namely the determinant of first order sequential principal minor is greater than 0. After the calculation, it can be found that the determinants of second and third order sequential principal minors are both greater than 0 shown as follows.

$$\begin{vmatrix}\varsigma_{p11} & \varsigma_{p12}\\ \varsigma_{p21} & \varsigma_{p22}\end{vmatrix}>0,\begin{vmatrix}\varsigma_{p11} & \varsigma_{p12} & \varsigma_{p13}\\ \varsigma_{p21} & \varsigma_{p22} & \varsigma_{p23}\\ \varsigma_{p31} & \varsigma_{p32} & \varsigma_{p33}\end{vmatrix}>0, \tag{19}$$

The determinant of the fourth order sequential principal minor is shown as follows.

$$\varsigma_{p11}\cdot\varsigma_{p22}\cdot\varsigma_{p33}\cdot\varsigma_{p44}-\varsigma_{p14}\cdot\varsigma_{p23}\cdot\varsigma_{p32}\cdot\varsigma_{p41}>0, \tag{20}$$

The range of c_1 can be obtained from Eq. (21).

$$c_1<\frac{2\varsigma_{p11}\cdot\varsigma_{p22}\cdot\varsigma_{p33}\cdot v_x}{\varsigma_{p23}\cdot\varsigma_{p32}\cdot x_{la}}, \tag{21}$$

The sum of yaw rate and lateral acceleration artificial potential field is shown in Eq. (22).

$$V_{\omega r}+V_{ay}=c_3(\frac{1}{\omega_\mu-\omega_r}-\frac{1}{\omega_\mu})^2+c_4(\frac{1}{a_{y\max}-a_y}-\frac{1}{a_{y\max}})^2, \tag{22}$$

Given the variables are in the denominator and $|\omega_r/\omega_\mu|\le 1$, the Taylor expansions are conducted for two terms shown in Eq. (23).

$$\begin{cases}V_{\omega r}=c_3(\frac{1}{\omega_\mu-\omega_r}-\frac{1}{\omega_\mu})^2\approx\frac{c_3\omega_r^{\,2}}{\omega_\mu^{\,4}}\\ V_{ay}=c_4(\frac{1}{a_{y\max}-a_y}-\frac{1}{a_y})^2\approx\frac{c_4a_y^{\,2}}{a_{y\max}^{\,4}}\end{cases}, \tag{23}$$

The derivative of $V_{\omega r}$ and V_{ay} can be given by Eq. (24).

$$\begin{cases}\dot{V}_{\omega r}=\frac{2c_3}{\omega_\mu^{\,4}}\omega_r\dot{\omega}_r\\ \dot{V}_{ay}=\frac{2c_4}{a_{y\max}^{\,4}}a_y\dot{a}_y\end{cases}, \tag{24}$$

After arrangement, the sum of the derivative of $V_{\omega r}$ and

V_{ay} can be obtained and be converted into matrix form as

$$\dot{V}_{\omega r}+\dot{V}_{ay}=-q_2^{\mathrm{T}}Qq_2, \tag{25}$$

where $q_2=\left[\dot{v}_y \quad \omega_r \quad v_y \quad \dot{\phi} \quad \phi \quad 1\right]^{\mathrm{T}}$ and the matrix Q is given as

$$Q=\begin{bmatrix} \xi_{q11} & \xi_{q12} & \mathrm{L} & \mathrm{L} & \mathrm{L} & \mathrm{L} \\ \xi_{q21} & \xi_{q22} & \mathrm{L} & \mathrm{L} & \mathrm{L} & \mathrm{L} \\ \mathrm{L} & \mathrm{L} & 0 & 0 & 0 & \mathrm{L} \\ \mathrm{L} & \mathrm{L} & 0 & 0 & 0 & \mathrm{L} \\ \mathrm{L} & \mathrm{L} & 0 & 0 & 0 & \mathrm{L} \\ \mathrm{L} & \mathrm{L} & \mathrm{L} & \mathrm{L} & \mathrm{L} & 0 \end{bmatrix}$$

with

$$\xi_{q11}=\frac{2c_4}{a_{y\max}{}^4}\frac{(k_1+k_2)I_{xeq}}{mI_xv_x},$$

$$\xi_{q22}=\frac{2c_3}{\omega_\mu{}^4}\frac{a^2k_1+b^2k_2}{I_zv_x}+$$

$$\frac{2c_4}{a_{y\max}{}^4}\left[\frac{(bk_2-\mathrm{a}k_1)(a^2k_1+b^2k_2)I_{xeq}}{mI_x{}^2v_x}+\frac{m_sh_g{}^2c(bk_2-\mathrm{a}k_1)}{mI_x{}^2}\right]$$

$$\xi_{q21}=\xi_{q12}=\frac{2c_4}{a_{y\max}{}^4}\left[\frac{(bk_2-\mathrm{a}k_1)(a^2k_1+b^2k_2)I_{xeq}}{mI_x{}^2v_x{}^2}\right.$$

$$\left.+\frac{m_sh_g{}^2c(bk_2-\mathrm{a}k_1)}{mI_x{}^2v_x}-\frac{(k_1+k_2)I_{xeq}}{mI_x}\right]$$

As long as the matrix Q is positive definite, $\dot{V}_{\omega r}+\dot{V}_{ay}$ will be less than 0. According to the form of matrix Q, it can be seen that the positive qualitative of matrix Q can be proved only by the first and second order sequential principal minor.

Just need to meet following conditions.

$$\xi_{q11}\cdot\xi_{q22}-\xi_{q12}{}^2>0, \tag{26}$$

To sum up, the Lyapunov stability of the control system is demonstrated under the conditions shown in Eq. (27) which are used for the constraints of controller parameters optimization.

$$\begin{cases} c_3>0 \\ c_4>0 \end{cases}\begin{cases} \xi_{q11}\cdot\xi_{q22}-\xi_{q12}{}^2>0 \\ c_1<\dfrac{2\varsigma_{p11}\cdot\varsigma_{p22}\cdot\varsigma_{p33}\cdot v_x}{\varsigma_{p23}\cdot\varsigma_{p32}\cdot x_{la}} \end{cases}, \tag{27}$$

4 Controller Parameters Optimization

4.1 Comprehensive Evaluation Index of Lane Keeping Control System

To evaluate the performance of lane keeping control system mentioned in this paper, a comprehensive evaluation index including path tracking accuracy and lateral stability is established. The evaluation indexes of path tracking accuracy include lateral deviation index and course deviation index. The evaluation indexes of lateral stability include the evaluation index of vehicle sideslip risk and the evaluation index of vehicle rollover risk[26-27].

The evaluation indexes of path tracking accuracy are given by following expressions.

$$J_{\mathrm{e}}=\int_0^{t_{\mathrm{n}}}\left[\frac{f(t)-y(t)}{E^*}\right]^2dt, \tag{28}$$

$$J_\varphi=\int_0^{t_{\mathrm{n}}}\left[\frac{\varphi(t)}{\varphi^*}\right]^2dt, \tag{29}$$

Where J_e is the lateral deviation index, J_φ is the course deviation index, $f(t)$ is the desired trajectory, $y(t)$ is the actual trajectory, E^* is the standard threshold value of trajectory error, t_{n} is the test time, $\varphi(t)$ is the actual heading angle, φ^* is the standard threshold value of heading angle deviation.

The evaluation indexes of lateral stability are given as follows.

$$J_\phi=\int_0^{t_{\mathrm{n}}}\left[\frac{\phi(t)}{\hat{\phi}}\right]^2dt, \tag{30}$$

$$J_{\mathrm{cf}}=\int_0^{t_{\mathrm{n}}}\left[\frac{F_{\mathrm{ZAf}}(t)/G_{\mathrm{ZAf}}}{\mu^*}\right]^2dt, \tag{31}$$

$$J_{\mathrm{cr}}=\int_0^{t_{\mathrm{n}}}\left[\frac{F_{\mathrm{ZAr}}(t)/G_{\mathrm{ZAr}}}{\mu^*}\right]^2dt, \tag{32}$$

$$J_{\mathrm{c}}=\max\left(J_{\mathrm{cf}},J_{\mathrm{cr}}\right), \tag{33}$$

where J_ϕ is the evaluation index of vehicle rollover risk,

$\phi(t)$ is the roll angle, $\hat{\phi}$ is the standard threshold value of vehicle rollover risk, J_c is the evaluation index of vehicle sideslip risk, J_{cf} is the evaluation index of sideslip risk of vehicle front axle, J_{cr} is the evaluation index of sideslip risk of vehicle rear axle, $F_{ZAf}(t)$ is the lateral force on the front axle of vehicle, $F_{ZAr}(t)$ is the lateral force on the rear axle of vehicle, $G_{ZAf}(t)$ is the load on the front axle of vehicle, $G_{ZAr}(t)$ is the load on the rear axle of vehicle, μ^* is the standard threshold value of vehicle sideslip risk.

Combining with Eq. (28) ~ Eq. (33), comprehensive evaluation index of lane keeping control system is given by

$$J=\sqrt{\frac{w_e J_e^{\ 2}+w_\varphi J_\varphi^{\ 2}+w_\phi J_\phi^{\ 2}+w_c J_c^{\ 2}}{w_e+w_\varphi+w_\phi+w_c}}, \tag{34}$$

where w_e is the weight coefficient of J_e, w_φ is the weight coefficient of J_φ, w_φ is the weight coefficient of J_φ, w_c is the weight coefficient of J_c. The weight coefficients of the above evaluation indexes are obtained by entropy weight method[28], which determines the index weight coefficients according to the amount of information provided by the observed values of each sub-index. Evaluation index data is obtained by Trucksim and Simulink co-simulation, with a sample size of 100 groups. The weight coefficients are calculated by following expressions and the results are shown as follows.

w_e =0.42, w_φ =0.13, w_ϕ =0.18, w_c =0.27.

4.2 Parameters Optimization based on AIWPSO algorithm

In order to obtain the optimal controller parameters, parameters optimization based on AIWPSO algorithm is carried out in which the comprehensive evaluation index and the range of controller parameters are taken as fitness function and optimization constraints respectively. Compared with PSO algorithm, AIWPSO algorithm has both global and local particle swarm search capabilities due to the adaptive inertia weight w with the environment as shown in Eq. (35).

$$w=\begin{cases} w_{\min}-\dfrac{(w_{\max}-w_{\min})\cdot(f-f_{\min})}{(f_{\text{avg}}-f_{\min})}, & f\le f_{\text{avg}} \\ w_{\max}, & f>f_{\text{avg}} \end{cases}, \tag{35}$$

Where $w_{\max}$ and $w_{\min}$ represent the maximum and minimum value of the inertia weight, f_{avg} and $f_{\min}$ represent the average and minimum fitness of all current particles.

In the algorithm, population size is set as 100 and the number of iterations is set as 100. The optimization iteration result is shown in Figure 4 in which Y-axis represents the fitness value and X-axis represents the number of iterations. By comparison, it is obvious that the convergence rate of AIWPSO is faster than that of PSO and the AIWPSO algorithm gets smaller fitness value. The optimal parameters based on AIWPSO algorithm are shown in Table 1.

Table 1 Controller parameters after optimization

Controller parameters	Value
c_1 / k_f	2.269
c_2 / k_f	0.354
c_3 / k_f	0.0078
c_4 / k_f	0.0013

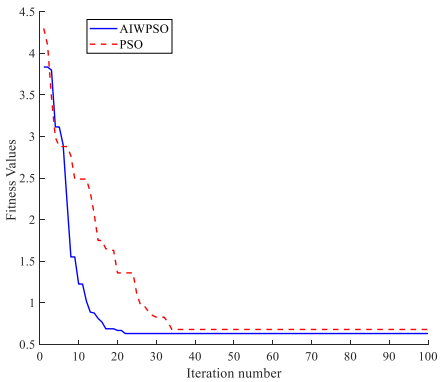

Figure 4 Optimization convergence curve

5 Simulation Analysis and Experimental Verification

5.1 Simulation Analysis of The Control Strategy

In order to verify the improved APF algorithm in lane keeping control of commercial vehicle, simulations on the Trucksim-Simulink platform are conducted under straight road condition and double lane change condition with initial deviation. The straight road condition with initial deviation is applied to validate the deviation correction ability of control algorithm. The double lane change condition including straight road and curve road is used to verify the trajectory tracking effect and lateral stability under comprehensive road condition. Besides, the control effect of the improved APF algorithm is compared with the single point pre-sighting driver model and traditional road APF algorithm.

Case 1: Lane keeping control simulation is conducted under straight road condition at the speed of 70 km/h. The initial lateral deviation is set as 0.5m. The results are shown in Figure 5.

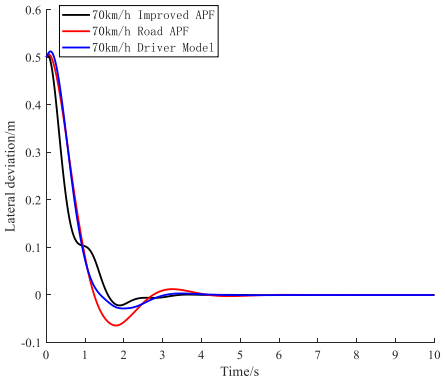

a) Lateral deviation

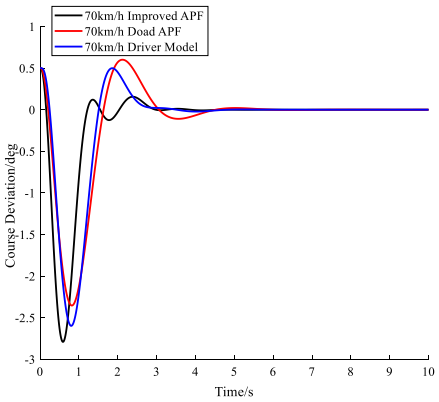

b) Course deviation

Figure 5 Lane keeping deviation under straight road condition at the speed of 70km/h

From the figures, it can be seen that the control effect under the improved APF algorithm is generally better than the single point pre-sighting driver model and the road APF algorithm. In Figure 5(a), the average lateral deviation under the improved APF algorithm is reduced by 14.46% and 20.85% respectively compared with the single point pre-sighting driver model and the road APF algorithm at the speed of 70 km/h. The peak overshoot of lateral deviation under the improved APF algorithm is 22.78% and 65.99% lower than the single point pre-sighting driver model and the road APF algorithm respectively. In Figure 5(b), the average course deviation under the improved APF algorithm is reduced by 22.77% and 31.62% by comparison respectively. It can be also found the course deviation under the improved APF algorithm achieves fast convergence to zero smoothly with smaller overshoot.

Case 2: Lane keeping control simulation is carried out under double lane change condition at the speed of 70 km/h. The path of double lane change condition is shown in Figure 6 and the results are shown in Figure 7.

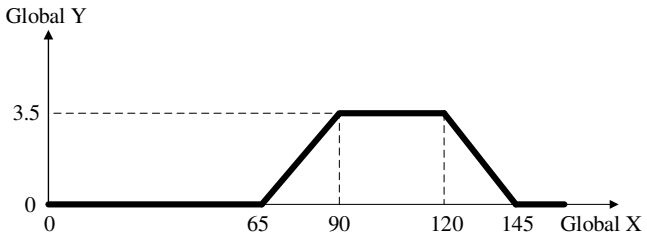

Figure 6 Path diagram of double lane change

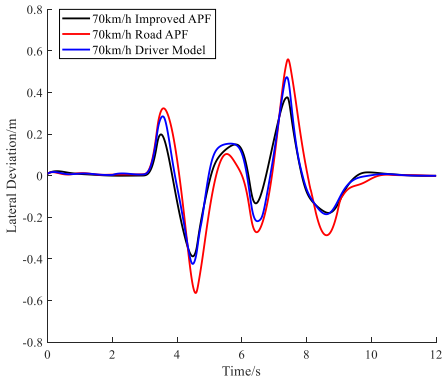

a) Lateral deviation

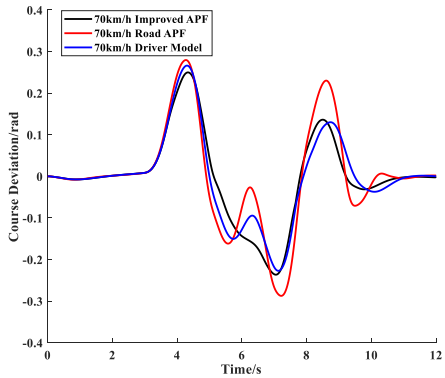

b) Course deviation

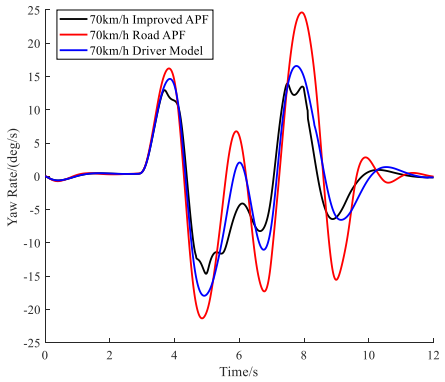

c) Yaw rate

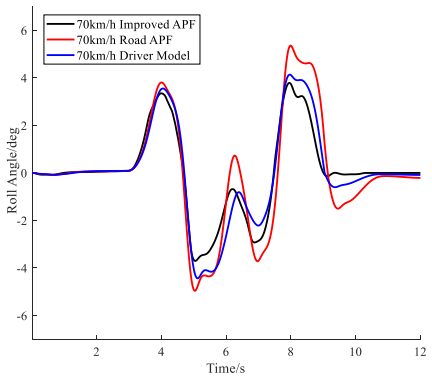

d) Roll angle

Figure 7 Comparison of control effect under double lane change condition at the speed of 70km/h

Under double lane change condition, four indicators are utilized to demonstrate the control effect of the improved APF algorithm, among which lateral deviation and course deviation represent the path tracking accuracy, yaw rate and roll angle represent the lateral stability of the vehicle. Among the three algorithms mentioned above, as shown in Figure 7, the fluctuating range of the indicators is largest under the road APF algorithm, which shows that the road APF algorithm may not meet the requirement of lane keeping control of commercial vehicles. In detail, in Figure 7 (a) and Figure 7 (b), the average lateral deviation under the improved APF algorithm is reduced by 21.27% and 10.68% compared with the road APF algorithm and the driver model, but the average course deviation is not the lowest compared with the road APF algorithm and the driver model, which may result from the compromise to the lateral stability. The evaluation index of path tracking is reduced by 18.73% and 7.08% by comparison respectively which demonstrates the improved APF algorithm has better performance in terms of tracking accuracy and the introduction of the TLC potential field in the controller is effective. From Figure 7 (c) and Figure 7 (d), it can be seen that the vehicle has the trend of instability under the road APF algorithm when the vehicle is driving at the sharp corner. In Figure 7 (c), yaw rate under the road APF algorithm is beyond the vehicle sideslip limitation of 20 deg/s at the time of 4.8s and 7.8s and the vehicle is in a great risk of sideslip. It is obvious that the improved APF algorithm has the remarkable effect on peak shaving of yaw rate, which decreases the risk of vehicle sideslip. Although the roll angle is under the limitation of vehicle rollover, the slightly high value affects the driving comfort. By calculation, the average peak of yaw rate is reduced by 45.16% and 18.63%, and average roll angle is reduced by 30.14% and 14.63% compared with the road APF algorithm and the driver model respectively. The evaluation index of lateral stability is reduced by 27.51% and 5.91%, which demonstrates the improved APF algorithm enhances the lateral stability significantly by introducing yaw rate and lateral acceleration into the potential field function. From the perspective of comprehensive evaluation index, the value is reduced by 23.4% and 6.5%, which reflects the improved APF algorithm improves the comprehensive performance of path tracking accuracy and lateral stability.

5.2 Experiment Verification of The Control Strategy

In order to verify the effectiveness of lane keeping control strategy based on the improved APF in the actual controller, the hardware in the loop (HiL) test for the proposed control strategy is carried out. The overall test scheme diagram is shown in Figure 8.

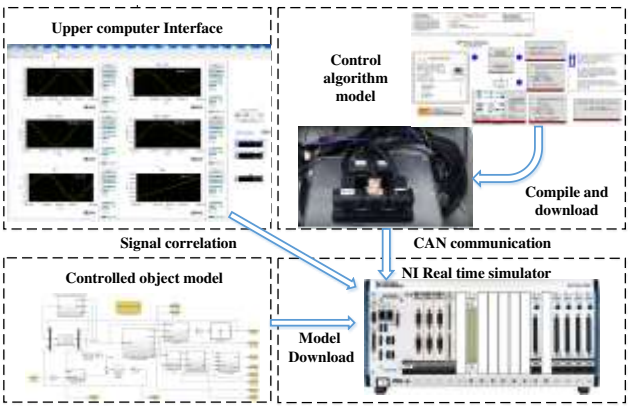

Figure 8 Diagram of HiL test scheme

The test is implemented under the double lane change condition at the speed of 70km/h. The HiL test results are

shown in Figure 9.

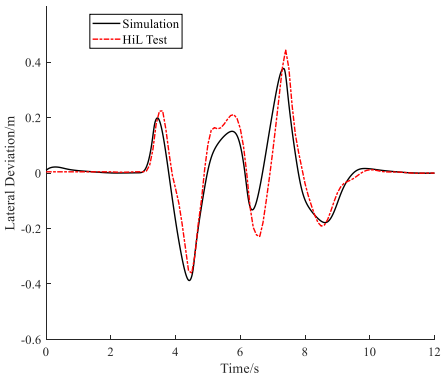

a) Comparison of lateral deviation

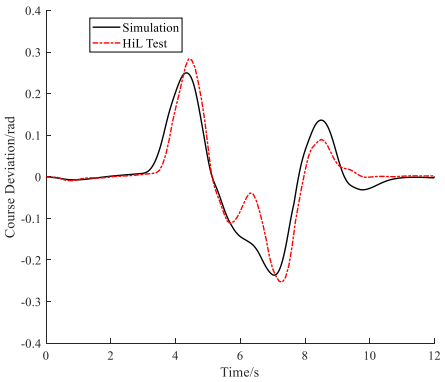

b) Comparison of course deviation

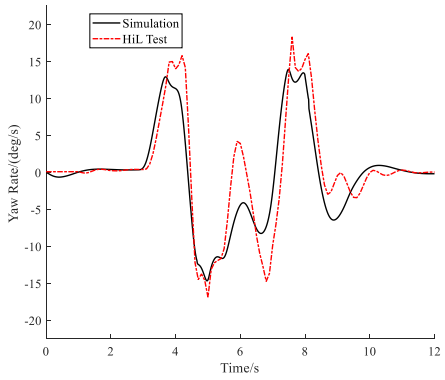

c) Comparison of yaw rate

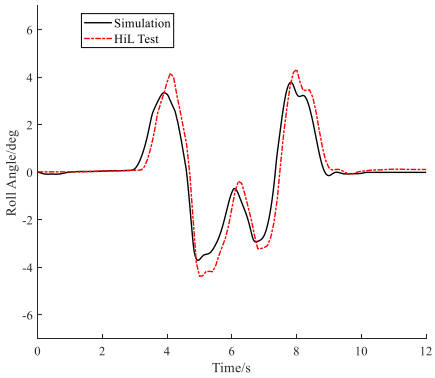

d) Comparison of roll angle

Figure 9 The results of HIL test

Figure 9 shows the comparison of lane keeping control effect between simulation and HiL test under double lane change condition. In Figures 9 (a) and 9 (b), it can be seen from the HiL test results, the lateral deviation increases to a certain extent, and the heading angle is adjusted when the vehicle completes the second large angle steering, but the driving path is basically the same with that in the simulation. In terms of lateral stability, Figures 9 (c) and 9 (d) show that the improved APF algorithm has a certain peak clipping effect on the yaw rate and roll angle at several sharp corners. Although the peak value has a certain increase, the increase range is small, and it does not exceed the stability limit, so as to ensure that it is in the state without instability.

In general, there are some differences between the HiL test results and simulation results in part which results from the delay and discrete setting of HiL test environment, but the differences are within the reasonable range and the trend of the observed variables in HiL test is basically consistent with that in simulation, which reflects the effectiveness and feasibility of the commercial vehicle lane keeping control based on the improved APF algorithm in the actual controller significantly.

6 Conclusion

The improved APF control algorithm is proposed for the lane keeping system in the commercial vehicle to achieve better path tracking accuracy and the lateral stability. Firstly, in this paper, the dynamics model of vehicle, the calculation model of TLC and the model of path tracking are constructed. Secondly, TLC, yaw rate and lateral acceleration are introduced into the traditional road artificial field function. Thirdly, the stability of the improved APF control system is proved based on

Lyapunov theory and the ranges of the controller parameters are determined. Fourthly, comprehensive evaluation index is established and the controller parameters are optimized based on AIWPSO algorithm. Finally, the simulations and HiL tests are carried out. From the results, it can be seen that the accuracy of path tracking is improved by increasing the TLC potential field. In terms of lateral stability, the introduction of yaw rate and lateral acceleration as repulsive force field not only guarantees the path tracking accuracy, but also improves the lateral stability especially under the condition of sharp corner tracking. In the future, we shall put more efforts in the improvement of dynamics models and attempt to investigate more advanced lane keeping system considering longitudinal dynamics of the vehicle.

7 Declaration

Acknowledgements

The authors sincerely thanks to Professor Hao-bin Jiang of Jiangsu University for his critical discussion and reading during manuscript preparation.

Funding

Supported by National Natural Science Foundation of China (Grant No. 51605199, and No. 51675235), Six Talent Peak Funding Projects in Jiangsu Province (Grant No.2019-GDZB-084), Special fund for the transformation of scientific and technological achievements in Taizhou (Grant No.SCG201904),and Key Science and Technology Support program in Taizhou (Grant No.TG202022).

Availability of data and materials

The datasets supporting the conclusions of this article are included within the article.

Authors' contributions

The author' contributions are as follows: ZL, ZX was in charge of the whole trial; BT and YY wrote the manuscript; HJ conceived and designed the research; ZH assisted with sampling and laboratory analyses. All authors read and approved the final manuscript

Competing interests

The authors declare no competing financial interests.

References

[1] K V Subramaniyam, S C Subramanian. Analysis of cornering response and stability of electrified heavy commercial road vehicles with regenerative braking. *Proceedings of the Institution of Mechanical Engineers Part D-Journal of Automobile Engineering*, 2019, 234(6): 1672-1689.

[2] T Q Zhou, J Y Zhang. Analysis of commercial truck drivers' potentially dangerous driving behaviors based on 11-month digital tachograph data and multilevel modeling approach. *Accident Analysis and Prevention*, 2019, 132: 105256.

[3] R L Hammond, S A Soccolich, R J Hanowski. The impact of driver distraction in tractor-trailers and motorcoach buses. *Accident Analysis and Prevention*, 2019, 126: 10-16.

[4] X J Han, W D Zhao, H Y Zheng, et al. Research on lane-keeping control strategy for bus. *International Journal of Heavy Vehicle Systems*, 2019, 26 (3-4): 291-314.

[5] A T Nguyen, C Sentouh, J C Popieul. Sensor reduction for driver-automation shared steering control via an adaptive authority allocation strategy. *IEEE-ASME Transactions on Mechatronics*, 2018, 23(1): 5-16.

[6] C Hu, Y C Qin, H T Cao et al. Lane keeping of autonomous vehicles based on differential steering with adaptive multivariable super-twisting control. *Mechanical Systems and Signal Processing*, 2019, 125: 330-346.

[7] Y G Bian, J Y Ding, M J Hu, et al. An advanced lane-keeping assistance system with switchable assistance modes. *IEEE Transactions on Intelligent Transportation Systems*, 2020, 21(1): 385-396.

[8] W Jeon, A Zemouche, R Rajamani. Tracking of vehicle motion on highways and urban roads using a nonlinear observer. *IEEE-ASME Transactions on Mechatronics*, 2019, 24(2): 644-655.

[9] J P Vasconez, D Carvajal, F A Cheein, On the design of a human-robot interaction strategy for commercial vehicle driving based on human cognitive parameters, *Advances in Mechanical Engineering*, 2019, 11(7).

[10] Y S Son, W Kim, S H Lee, et al. Robust multirate control scheme with predictive virtual lanes for lane-keeping system of autonomous highway driving. *IEEE Transactions on Vehicular Technology*, 2014, 64(8): 3378-3391.

[11] W W Chen, L F Zhao, H R Wang, et al. Parallel distributed compensation/h(infinity)control of lane-keeping system based on the takagi-sugeno fuzzy model. *Chinese Journal of Mechanical Engineering*, 2020, 33(1): 1-13

[12] Z Li, G J Cui, S S Li, et al. Lane keeping control based on model predictive control under region of interest prediction considering vehicle motion states. *International Journal of Automotive Technology*, 2020, 21(4): 1001-1011.

[13] C Hu, Z F Wang, Y C Qin, et al. Lane keeping control of autonomous vehicles with prescribed performance considering the rollover prevention and input saturation. *IEEE Transactions on Intelligent Transportation Systems*, 2020, 21(7): 3091-3103.

[14] H B Wang, W Cui, Z Xia, et al. Vehicle lane keeping system based on TSK fuzzy extension control. *Proceedings of the Institution of Mechanical Engineers Part D-Journal of Automobile Engineering*, 2020, 234(2-3): 762-773.

[15] Y Rasekhipour, A Khajepour, S K Chen, et al. A potential field-based model predictive path-planning controller for autonomous road vehicles, *IEEE Transactions on Intelligent Transportation Systems*, 2017, 18(5): 1255-1267.

[16] U Orozco-Rosas, O Montiel, R. Sepulveda. Mobile robot path planning using membrane evolutionary artificial potential field, *Applied Soft Computing*, 2019, 77: 236-251.

[17] E J Rossetter, J C Gerdes. Lyapunov based performance guarantees for the potential field lane-keeping assistance system, *Journal of Dynamic Systems Measurement and Control-Transactions of the*

ASME, 2006, 128(3): 510-522.
[18] Q D Wang, Z Y Wei, W W Chen, et al. Lane keeping coordination control based on parameter-varying artificial potential field, *Journal of Mechanical Engineering*, 2018, 54(18): 105-114. (in Chinese)
[19] Y Marumo, T Yokota, A Aoki. Improving stability and lane-keeping performance for multi-articulated vehicles using vector follower control, *Vehicle System Dynamics*, 2020, 58(12): 1859-1872.
[20] A S Trigell, M, Rothhamel, J Pauwelussen, et al. Advanced vehicle dynamics of heavy trucks with the perspective of road safety, *Vehicle System Dynamics*, 2017, 55(10): 1572-1617.
[21] A A Nagra, F Han, Q H Ling. An improved hybrid self-inertia weight adaptive particle swarm optimization algorithm with local search, *Engineering Optimization*, 2019, 51(71): 115-1132.
[22] T Chen, L Chen, X Xu, et al. Passive fault-tolerant path following control of autonomous distributed drive electric vehicle considering steering system fault, *Mechanical Systems and Signal Processing*, 2019, 123: 298-315.
[23] Y J Huang, H T Ding, Y B Zhang, et al. A motion planning and tracking framework for autonomous vehicles based on artificial potential field elaborated resistance network approach. *IEEE Transactions on Industrial Electronics*, 2020, 67(2): 1376-1386.
[24] W Z Zhao, X X Qin, C Y Wang. Yaw and lateral stability control for four-wheel steer-by-wire system. *IEEE-ASME Transactions on Mechatronics*, 2018, 23(6): 2628-2637.
[25] L Liu, S H Ding, L Ma, et al. A novel second-order sliding mode control based on the Lyapunov method. *Transactions of the Institute of Measurement and Control*, 2019, 41(4): 1068-1078.
[26] S D Liu, Z S Hou, T T Tian, et al. Path tracking control of a self-driving wheel excavator via an enhanced data-driven model-free adaptive control approach. *IET Control Theory and Applications*, 2020, 14(2): 220-232.
[27] W L Zhang, L Drugge, M Nybacka, et al. Active camber for enhancing path following and yaw stability of over-actuated autonomous electric vehicles, *Vehicle System Dynamics*, 2021, 59(5): 800-821.
[28] M Muqeem, A F Sherwani, M Ahmad, et al. Application of the Taguchi based entropy weighted TOPSIS method for optimisation of diesel engine performance and emission parameters. *International Journal of Heavy Vehicle Systems*, 2019, 26(1): 69-94.

Biographical notes

Bin Tang received the B.S. degree in electronics and information engineering, and the M.S. and Ph.D. degrees in vehicle engineering from *Jiangsu University*, *Zhenjiang*, *China*, in 2007, 2011, and 2015, respectively. He is currently an associate professor with the *Automotive Engineering Research Institute*, *Jiangsu University*. His research interests include vehicle handling dynamics and control, intelligent steering, electric motor drive and control.
Tel: 0511-88782845; E-mail: tangbin@ujs.edu.cn

Zheng-Yi Yang received the B.S. degree in traffic equipment and control engineering from *Nantong University*, *Nantong*, *China*, in 2020. She is currently a postgraduate student in the *Automotive Engineering Research Institute*, *Jiangsu University*, majored in vehicle engineering. Her research interest is lane keeping control.

Hao-Bin Jiang received the B.S. degree from *Nanjing Agricultural University*, *Nanjing*, *China*, in 1991, and the M.S., and Ph.D. degrees from *Jiangsu University*, *Zhenjiang*, *China*, in 1994 and 2000, respectively, all in mechanical engineering. He is currently a professor with the *School of Automotive and Traffic Engineering*, *Jiangsu University*. His research interests include vehicle dynamics performance analysis and electronic control technologies for vehicles.

Zi-Yan Lin received the B.S. degree in vehicle engineering from *Jiangsu University*, *Zhenjiang*, *China*, in 2018. He is currently a postgraduate student in the *Automotive Engineering Research Institute*, *Jiangsu University*, majored in vehicle engineering. His research interest is intelligent steering control.

Zhan-Xiang Xu received the B.S. degree in vehicle engineering from *Anhui University of Science and Technology*, *Huainan*, *China*, in 2019. He is currently a postgraduate student in the *Automotive Engineering Research Institute*, *Jiangsu University*, majored in vehicle engineering. His research interest is path planning and tracking.

Zi-Tian Hu received the B.S. degree in vehicle engineering from *Nanhang Jincheng College*, *Nanjing*, *China*, in 2020. He is currently a postgraduate student in the *Automotive Engineering Research Institute*, *Jiangsu University*, majored in vehicle engineering. His research interest is intelligent vehicle decision-making and planning.